Feedforward and Feedback Control of a Flexible Robotic Arm

Robert L. Wells, John K. Schueller, and Jiri Tlusty

ABSTRACT: Feedforward and feedback control strategies are applied to a servo-driven flexible structure and studied in time-domain computer simulations. Simulation results are compared to experimental runs on a flexible arm apparatus. The most accurate and stable responses of the arm are obtained by adding corrective terms to the command signals when position feedback is taken only from the servo. Full conditioning of the command signal, which involves compensating for the dynamics of both the servo and the arm, produced the best response. Simulations and experiments show that positional and accelerometric feedback, as combined with a proportional-derivative element acting on the position error, is a viable solution in the less stable situation when feedback is being taken only from the manipulator.

Introduction

When a servomotor drives a flexible structure, the structure's natural frequencies, as compared to the bandwidth of the servo-drive, determine the contribution of the structural flexibility to the errors of the resulting motion. In current industrial robots, the drives are often relatively slow and the structures are relatively rigid, so that overshoots and other errors are caused mainly by the servodrive. However, depending on the accuracy required, the structural deflections of the driven members may become significant. Structural flexibility must be considered the major source of motion errors in space structures and manipulators [1]. Because of weight restrictions in space, large arm lengths result in flexible structures. Furthermore, future industrial robots should require lighter and more flexible manipulators. References [2]–[4] contain good overviews of research in the area of flexible robotic manipulators.

To investigate the effects of structural flexibility and how different control schemes can reduce unwanted oscillations, an experimental apparatus was constructed consisting of a DC servomotor driving a slender aluminum beam. The purpose of the experiments was to identify simple and effective control strategies to deal with the motion errors that occur when a servomotor is driving a very flexible structure. Time-domain simulations were developed to model the behavior of the servo and the arm, and were compared to the experimental results. Since robot controllers have extensive computational overhead, emphasis was placed on using the simplest linear models of the servo and the arm that still predicted the motions accurately.

Two kinds of control strategy were investigated. In the first, the motion command signal was used to compensate for the dynamics of the positional servo and the arm. No position feedback was taken from the arm tip. This is often referred to as feedforward control [5], [6]. In the second approach, compensators were used in a feedback configuration, with the arm tip location fed back to the motor controller and the motor operated as a velocity servo. There are other, more sophisticated, control strategies, but they were not considered here. In addition, note that the feedforward strategy has its limitations. The controller cannot know if the arm has reached the target, and there is no allowance for disturbance rejection.

Modeling Servo and Flexible Arm

The experimental apparatus consisted of an armature-controlled DC servomotor driving a 25.4-mm × 3.175-mm 6061-T6 aluminum arm in the horizontal plane. The effective length of the arm was 743 mm. Gear reduction was through a 100:1 harmonic drive. Position feedback from the drive was from a precision potentiometer, and the arm deflection was sensed using a strain gauge mounted at the root of the arm. A piezoelectric accelerometer was mounted at the end of the arm, and its signal was integrated numerically to obtain velocity. A microcomputer with a 12-bit analog-to-digital (A/D)/digital-to-analog (D/A) board was used to implement the control laws. Figures 1 and 2 show the experimental apparatus and the system wiring diagram, respectively. The Table presents a list of the physical parameters that describe the servomotor and the arm.

Servomotor

An armature-controlled permanent magnet DC servomotor of the type typically used on industrial robots was used in the experiments. It can be represented as a first-order system with gain K_m and a mechanical time constant τ_m. The electrical time constant, due

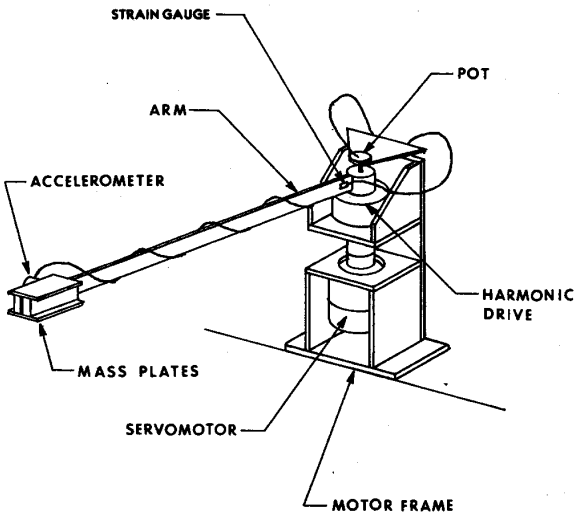

Fig. 1. Experimental apparatus.

Robert L. Wells, John K. Schueller, and Jiri Tlusty are with the Department of Mechanical Engineering, University of Florida, Gainesville, FL 32611.

0272-1708/90/0100-0009 $01.00 © 1990 IEEE

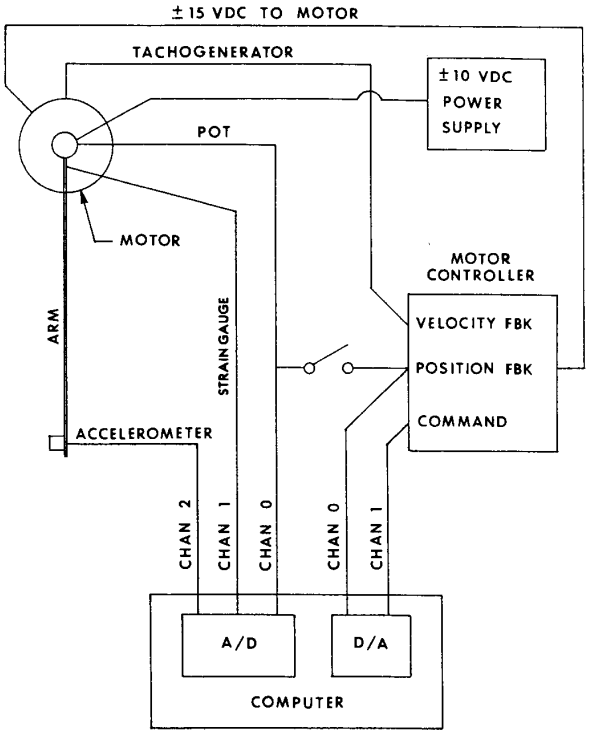

Fig. 2. Wiring diagram.

Table
Parameters of Servo and Arm

Servo time constant τ_d, sec	0.005
Overall servo gain $G = K_p K_d r$ (1/sec)	3.40
Positional servo frequency ω_d, Hz	4.15
Positional servo damping ζ_d	3.83
Reflected arm mass plus payload, kg	0.60
Spring constant of arm, N/m	33.0
Arm natural frequency ω_a, Hz	1.18
Arm damping ratio ζ_a	0.01

to the inductance of the armature, and the effect of friction losses were neglected. The whole system was taken as linear, although, in reality, there is always a limit on armature current, or on torque.

Servomotors typically are used with tachogenerator feedback. The tachogenerator coefficient is H (V/rad/sec). The feedback voltage $H\omega$ is subtracted from the velocity command voltage v_c and preamplified by K_a. This type of servo is rather insensitive to the load torque due to the typically large value of K_a amplifying the velocity error. This allows any effect on ω from the driven arm's torque to be neglected. The differential equation that describes the servomotor with velocity feedback follows.

$$\tau_d \dot{\omega} + \omega = K_d v_c \qquad (1)$$

where

$$\tau_d = \tau_m/(1 + K_a K_m H)$$

$$K_d = K_a K_m/(1 + K_a K_m H)$$

Equation (1) shows that the whole drive system of the servomotor with the tachogenerator feedback can be represented by a first-order system with the closed-loop time constant of the drive τ_d and the closed-loop gain of the drive K_d. In most instances, τ_d and K_d are sufficient to represent the drive without considering the internal parameters.

When position commands are sent to the drive, a feedback loop may be closed around the servomotor by locating a positional transducer on the shaft of the motor. The output angle is transformed by the transmission ratio r into a position x, which is fed back and compared to the commanded position x_c. The error of position, e_p, is amplified by the positional gain, K_p, and converted to analog form producing the command input, v_c, to the servodrive. The corresponding transfer function is obtained as shown, where $G = K_p K_d r$ is the overall gain of the servo.

$$X(s)/X_c(s) = G/(\tau_d s^2 + s + G) \qquad (2)$$

Equation (2) can also be expressed as

$$X(s)/X_c(s) = \omega_d^2/(s^2 + 2\zeta_d \omega_d s + \omega_d^2) \qquad (3)$$

It can be seen that a second-order system is obtained, with a natural frequency ω_d and a damping ratio ζ_d. Equation (3) can also be written as a time-domain differential equation:

$$\ddot{x} + 2\zeta_d \omega_d \dot{x} + \omega_d^2 x = \omega_d^2 x_c \qquad (4)$$

where

$$\omega_d = (G/\tau_d)^{1/2}$$

$$\zeta_d = 1/[2(G\tau_d)^{1/2}]$$

Flexible Arm

A good account of the verification of a linear model of a flexible manipulator may be found in [7], where research demonstrates that the vibrations in a servo-driven flexible arm are best described by a clamped-free cantilever beam (as opposed to a pinned-free beam). The clamped-free model was adopted for the present research.

The equations for the arm can be derived by representing it as a single-degree-of-freedom (SDOF) vibrating system (Fig. 3). This simplification was adopted because it was an objective of this research to show that most motion errors can be largely eliminated if only the first vibrational mode of the arm is controlled.

The free transverse vibration of a uniform cantilever beam is expressed by the Bernoulli-Euler equation, where E is the elastic modulus, I the area moment of inertia, $\overline{m}$ the mass per unit length, x the beam's longitudinal direction, $v(x, t)$ the transverse motion of a point on the neutral axis of the beam, and t the time.

$$EI(\partial^4 v/\partial x^4) + \overline{m}(\partial^2 v/\partial t^2) = 0 \qquad (5)$$

The fundamental assumption in this equation is that deflections due to both the transverse

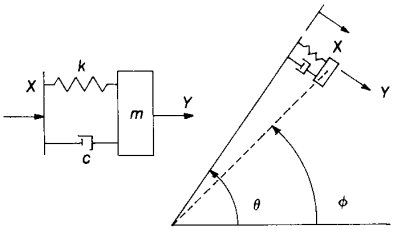

Fig. 3. Flexible arm model.

shear forces in the beam and the rotary inertia forces acting on a cross section are small and may be neglected. This assumption is valid for long, slender beams. The solution of Eq. (5) leads to expressions for the natural frequencies, ω_i, of the beam, where L is the length of the beam.

$$\omega_i = (\lambda_i L)^2[EI/(\bar{m}L^4)]^{1/2} \qquad (6)$$

For the first vibrational mode of a cantilever beam, the value of $(\lambda_1 L)$ is 1.8751 (see [8]). From basic mechanics of materials, the spring constant of the first mode of a cantilever can also be expressed as

$$k = 3EI/L^3 \qquad (7)$$

The mass of the beam reflected in the first mode of vibration is equal to the spring constant, defined in Eq. (7), divided by the square of the first natural frequency, defined in Eq. (6).

The total mass, m, of the beam model will be the reflected mass, m_r, plus any payload mass concentrated at the end of the beam, M.

$$m = m_r + M = k/\omega_1^2 + M \qquad (8)$$

The damping of structures can sometimes be difficult to determine. Tlusty and Stern [4] estimate that a damping ratio in the range of 1–4 percent is typical of machine members such as robot arms. The experimental arm was observed to be damped lightly, with a value of $\zeta_a \approx 1$ percent.

As shown in the schematic representation of Fig. 3, the input to the arm system is the angle of rotation of the motor shaft through a transmission θ, and the output is the angle of rotation of the arm ϕ. The rotating system may be considered analogous to a translatory system with input x and output y. The transverse displacement, y, of the arm tip can be related to an imaginary link that represents the angular arm tip position ϕ. The curvilinear trajectory of the arm, y, would then be obtained by converting from the rotational to the translatory system using the mensuration formula $y = L\phi$, where L is the effective length of the beam. This approach allows the arm parameters to be applied directly as derived from the beam equations.

The arm has a mass m, a spring with stiffness k, and a dashpot with a damping coefficient c. Summing forces on the mass gives the equation of motion of the arm,

$$m\ddot{y} + c\dot{y} + ky = c\dot{x} + kx \qquad (9)$$

where

$$c = \zeta_a^2(km)^{1/2}$$

It can be seen that Eq. (9) represents a base excited system and leads to the transfer function that relates the servo output to the arm output. The transfer function, where $\omega_a = (k/m)^{1/2}$ is the undamped first natural frequency of the arm model, can be written in an equivalent form as $F(s)$.

$$Y(s)/X(s) = F(s) = [1 + 2(\zeta_a/\omega_a)s] \cdot [\omega_a^2/(s^2 + 2\zeta_a\omega_a s + \omega_a^2)] \qquad (10)$$

System Model

The dynamics of the overall system depend on how position feedback is taken. If the feedback is taken from the servo only, then the situation lends itself to feedforward control. The system transfer function relates the arm output, y, to the command function, y_c.

$$Y(s)/Y_c(s) = [\omega_d^2/(s^2 + 2\zeta_d\omega_d s + \omega_d^2)]F(s) \qquad (11)$$

If there is position feedback from the arm only, the transfer function is more complicated. For this case, the flexibility of the arm is enclosed within the control loop, and as the value of G is increased the system will become unstable. In order to simulate the flexible arm response to the servo motion for this arrangement, Eq. (9) can be solved numerically to yield the arm tip position y.

Feedforward Compensation

The feedforward control strategies studied in the present research were obtained by conditioning the motion command signal to compensate for the dynamics of the servo and the manipulator. In these schemes, the flexible arm was driven by a positional servomotor with no position feedback taken from the arm.

The position command functions used to drive the arm were a quadratic spline command profile and a polynomial command profile. The quadratic spline, which has a trapezoidal velocity profile, is a common command signal used in robot arms [5], [9]. The polynomial was included as an example of how command functions that have continuous higher time derivatives can improve the arm performance in their own right. In addition, it will result that the smoother acceleration profiles of these commands enhance the effectiveness of the command signal conditioning schemes.

Simple Correction

The system response to the quadratic spline without any correction was studied first. The quadratic spline was formulated such that a constant acceleration of 120 deg/sec^2 was commanded for 0.25 sec, then a constant velocity of 30 deg/sec was commanded for 1.25 sec. Finally, a deceleration of 120 deg/sec^2 was commanded for another 0.25 sec. The net position command is to go from 0 to a final value of 45 deg in 1.75 sec. The polynomial command used the same final value and total command time as the quadratic spline.

The simulated response to the quadratic spline is plotted in Fig. 4, and is confirmed by the actual response shown in Fig. 5. Note that the linear servo model and SDOF model of the arm used in the simulation have adequately captured the system dynamics. A steady-state error, or "velocity lag," is evident in the servo response, x, as it follows the position command. The error is computed to be $E_{ss} = 30/G = 8.8$ deg. The drive, due to its high damping, does not overshoot, but the arm, y, overshoots by about 3.0 deg and continues to oscillate due to its low estimated damping ratio of $\zeta_a = 0.01$.

The simple feedforward correction to the command signal is derived by requiring that the resulting arm motion, y, follows exactly the servo output, x. Here, the dynamics of the servo are neglected. An additional corrective term is identified and added to the command, which compensates for the lags and transients of the arm. Neglecting the servo dynamics implies that the servo output, x, will follow exactly the command signal, y_c. After this substitution, Eq. (9) is solved for y_c.

$$y_c = (m/k)\ddot{y} + (c/k)\dot{y} + y - (c/k)\dot{y}_c \qquad (12)$$

The second assumption made for the simple corrective term is that the very low damping of flexible arms compared to their stiffness allows the terms multiplied by c/k to be neglected. Since arm output y ideally should follow the command signal, let $y = y_c$ and define a new corrected command signal y_{cor}. This is the command function with the *simple correction*.

$$y_{cor} = (m/k)\ddot{y}_c + y_c \qquad (13)$$

The corrective term is seen to be $(m/k)\ddot{y}_c$. Referring to Fig. 3, it is seen that the corrective term consists of the force ma, required to overcome the inertia of the mass, divided by the stiffness k of the spring. At the beginning of the motion, the corrective term gives an extra boost to the command signal to compress the spring initially. When the command is decelerating, the correction retards the motion of the arm in the same way.

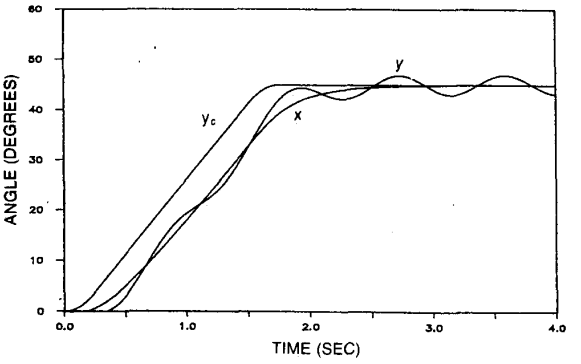

Fig. 4. Simulated response to quadratic spline.

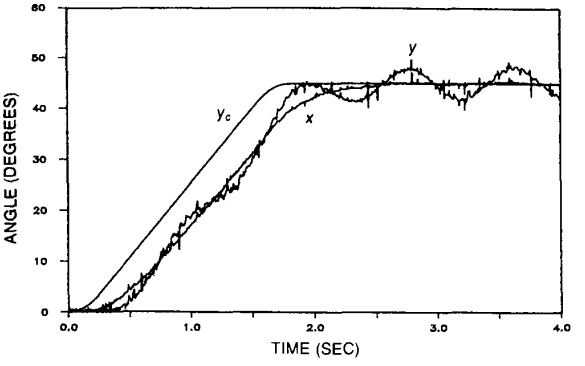

Fig. 5. Actual response to quadratic spline.

The results of the experimental run are shown in Fig. 6. The effect of the conditioning on the command signal is clearly evident. The effect on the servo is less apparent due to its high damping of $\zeta_d = 3.83$, but it causes the arm to follow the servo trajectory, as expected. The final value of 45 deg is reached in 2.5 sec with almost no overshoot. The effectiveness of the simple correction is seen clearly when Fig. 6 is compared to the uncorrected result shown in Fig. 5.

In addition to the quadratic spline, the response of the system to a polynomial position command was also studied. The polynomial command function was a fifth-degree expression of the following form (where $c_3 = 10\, y_f/t_c^3$, $c_4 = -15\, y_f/t_c^4$, and $c_5 = 6\, y_f/t_c^5$):

$$y_c = c_3 t^3 + c_4 t^4 + c_5 t^5 \qquad (14)$$

The term y_f is the final value of the command function (45 deg), and t_c is the command time (1.75 sec). The design of motion specifications such as this polynomial is described by Tesar and Matthew [10].

The response of the system to the uncorrected polynomial command is shown in Fig. 7. The first feature to notice is that the arm follows the servo with much less oscillation than in the response to the uncorrected quadratic spline shown in Fig. 5. This is because the command function is continuous in acceleration, in contrast to the quadratic spline, which is stepwise in acceleration. For this case, when the simple corrective term was added, only a slight reduction of the arm vibration was observed.

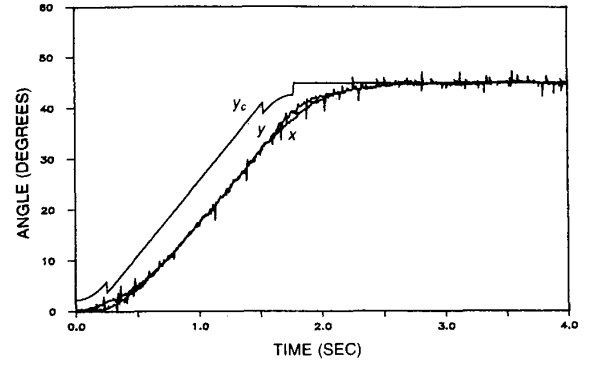

Fig. 6. Response to quadratic spline with simple conditioning.

Full Correction

In order to find the command function y_{cor} that would compensate for the dynamics of both the servo and the arm, a time-domain computer simulation was used to generate the fully corrected command signal numerically. Referring again to Eq. (9), the differential equation of the arm can be solved explicitly for the servo velocity $\dot{x}$.

$$\dot{x} = [m\ddot{y} + c\dot{y} + ky - kx]/c \qquad (15)$$

Equation (15) can be differentiated numerically to give $\ddot{x}$ and integrated to give the servo output x. The motion profile of the arm, y, would be the command function y_c, which describes the desired motion of the arm.

The differential equation of the positional servomotor, Eq. (4), can be solved for a command function y_{cor}, which will give the necessary servo response x.

$$y_{cor} = \ddot{x}/\omega_d^2 + \dot{x}(2\zeta_d/\omega_d) + x \qquad (16)$$

Note that the acceleration, velocity, and position of the servo already have been obtained from Eq. (15). Given the desired arm motion function $y = f(t)$ and its first two time derivatives, Eqs. (15) and (16) now can be combined in a computer program and solved numerically to obtain the command function with *full correction*.

Figure 8 shows the experimental run of the fully conditioned polynomial command. The effect of the conditioning is seen to raise the command profile dramatically. The arm response is smooth and accurate, as was the case with the simple conditioning, although the excitation of a higher mode is evident. The main difference is that the arm now follows almost exactly the desired motion profile and reaches its final value of 45 deg in the commanded time of 1.75 sec. This is a significant time improvement over the uncorrected polynomial command.

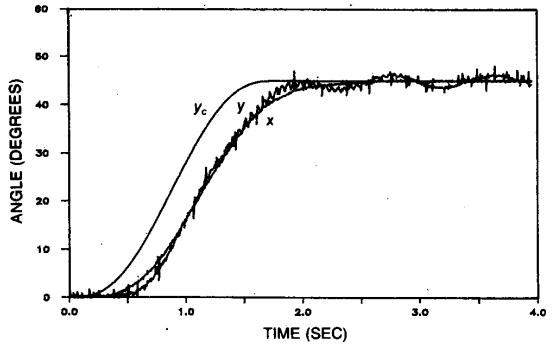

Fig. 7. Response to polynomial.

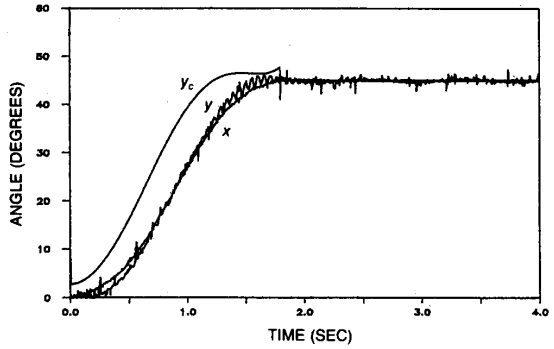

Fig. 8. Response to polynomial with full conditioning.

Feedback Control

In the feedback control schemes described next, the position of the arm tip was fed back to the servomotor controller. No position feedback was taken from the servo.

Stability Analysis

The arm tip position was obtained in the experiments by summing the scaled signals of a precision potentiometer located at the output of the harmonic drive and a strain gauge located at the root of the arm immediately adjacent to the hub. However, the spring-mass-dashpot system is now included in the feedback loop. This results in a much less stable system. Stabilizing elements now must be included either in the feedback path or in the forward path of the control loop.

In order to select the appropriate stabilizing elements, a stability analysis in the frequency domain using the Nyquist criterion was performed. After insight into the character of the system was gained, compensating terms were designed to raise the phase angle and guarantee stability. Denoting the individual terms as a, b, c, and d, the open-loop transfer function of the system can be written as

$$Y(s)/Y_c(s) = \underbrace{[G/(1 + \tau_d s)]}_{\text{(a)}}\underbrace{(1/s)}_{\text{(b)}} \cdot \underbrace{[\omega_a^2/(s^2 + 2\zeta_a\omega_a s + \omega_a^2)]}_{\text{(c)}} \cdot \underbrace{[1 + 2(\zeta_a/\omega_a)s]}_{\text{(d)}} \quad (17)$$

Figure 9 shows a plot of the magnitudes of the individual elements and the overall system on a log-log scale. Figure 10 shows a plot of the individual elements and the total system phase on a semilog scale. For τ_d = 0.005 sec, the first-order term (a) has a corner frequency of $1/\tau_d$ = 200 rad/sec. Term b, which is a pure integration, shifts the phase by −90 deg over the whole frequency range. The natural frequency of the third term (c) is ω_a = 1.18 Hz = 7.42 rad/sec. The corner frequency of the lead term (d) from the interface between the servo and the arm is $\omega_a/(2\zeta_a)$ = 371 rad/sec.

The phase diagram shows that the negative phase from the servo (a) and the stabilizing positive phase from the lead term (d) are not significant at low frequencies. The phase of the arm (c) changes very abruptly at ω_a because of the low arm damping ratio. When the phase of term c is added to that of term b, it can be seen that the critical frequency, ω_L, at which the system phase (P) passes −180 deg is close to ω_a. The magnitude (M) of the transfer function at this point is dictated again by the terms b and c, and it is found that at $\omega_L \approx \omega_a$ the magnitude is approximately $|M|$ = 6.5 and the critical value of the system gain at the limit of stability is G_L = 0.15. With this low gain, the stable system is very sluggish.

Double Lead Compensation

By observing the phase plot in Fig. 10, it is obvious that the system phase (P) must be raised at a frequency below ω_a. A double lead compensator was selected to be applied in the feedback loop. The effect of this element is to raise the phase of the system 180 deg over the frequency range, with 90 deg of phase having been added at its corner frequency. The expression for this compensator can be written as

$$(1 + as)^2 = 1 + 2as + a^2s^2 \quad (18)$$

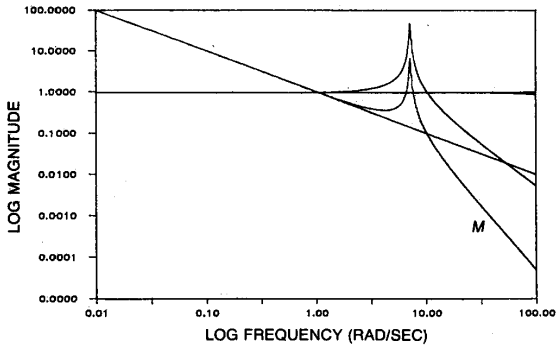

Fig. 9. Magnitude plot.

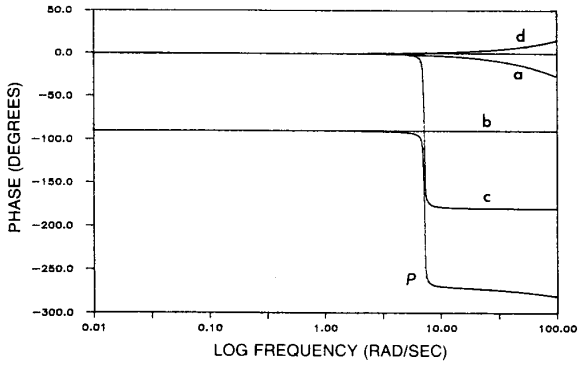

Fig. 10. Phase plot.

A corner frequency of 5.0 rad/sec was chosen to be below the critical frequency of $\omega_a = 7.42$ rad/sec. This gives the value of the coefficient to be $a = 1/5 = 0.2$. The least value of phase is now approximately -150 deg at $\omega = 8$ rad/sec. The acceleration in the a^2s^2 term was obtained from an accelerometer, and the velocity feedback in the $2as$ term was obtained by numerically integrating the acceleration.

Figure 11 presents the response of the compensated feedback scheme to a position ramp command, which requires the arm to be at 45 deg in 1.5 sec. Stability is achieved with $G = 3.4$, and the arm sweeps smoothly to target. However, the $2as$ term from Eq. (18) in the feedback adds a large velocity lag of approximately 15 deg to the response. Consequently, the arm barely has reached the target after 4 sec. Since the purpose of designing lightweight, flexible manipulators is, in part, to increase the speed of response, and since velocity lags are known to create motion errors in multiple coordinate manipulators [4], the nature of this response is not as good as it may appear at first.

P-D Correction in the Forward Path

Because it is the velocity term of the double lead compensator that has caused the excessive velocity lag, the next approach is to place an equivalent proportional-derivative (P-D) term in the feedforward path and remove the velocity term from the feedback path. The feedback will be left with what is called a P-D^2 term (see the block diagram of Fig. 12). The effect of the acceleration term is to increase the system phase by 180 deg at its corner frequency of 5 rad/sec. This element contributes to the stability of the system, and its value from the previous case will be retained.

$$\text{P-D}^2 = 1 + a_2s^2 = 1 + 0.04s^2 \quad (19)$$

The P-D compensator in the forward path contributes a 90-deg phase shift over the frequency range, with 45 deg of phase having been added at its corner frequency. It can be seen from Fig. 12 that this compensation is applied to the positional error term, ERP, in the forward path of the control loop. The velocity lag of the system response now can be reduced by selecting a smaller value for the velocity coefficient than was used in the double lead strategy. For this case, the P-D compensator block was selected to have the same corner frequency as the P-D^2 term.

$$\text{P-D} = 1 + a_1s = 1 + 0.2s \quad (20)$$

The separation of the terms has added more phase to the system, thereby allowing reduction of the velocity coefficient. The response of the servo and arm to the ramp command is plotted in Fig. 13. What is immediately evident is that the velocity lag has been reduced significantly, as was expected. The arm now reaches the target in less than 3 sec, although there is some continuing vibration evident. Further improvement is possible, but the plot also suggests that, since sensor data describing the servo and arm behavior are now inside the control loop, unmodeled nonlinearities in the drive, such as backlash and slip-stick friction, will cause less agreement between the simulation and the experimental results.

Conclusions

The best results regarding the accurate and stable response of the flexible arm were obtained by adding corrective terms to the command signals. The simulations and experiments showed that positional and accelerometric feedback, combined with a proportional-derivative compensator acting on the position error, was a viable solution in the less stable situation when feedback was taken only from the manipulator.

It was confirmed that a linear model of the servomotor, in combination with a single-

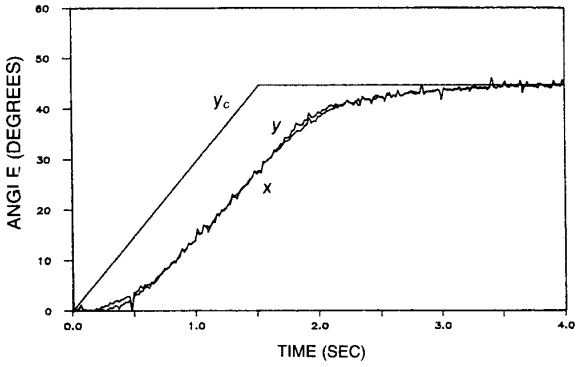

Fig. 11. Response of double lead system.

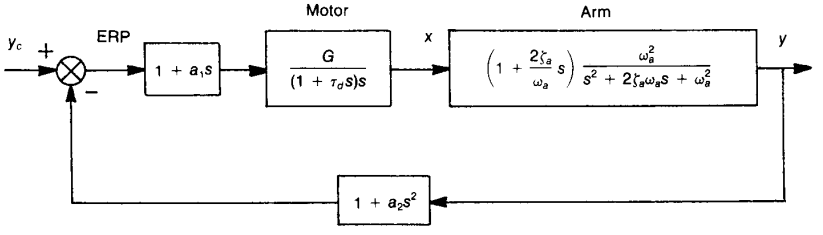

Fig. 12. P-D correction in forward path.

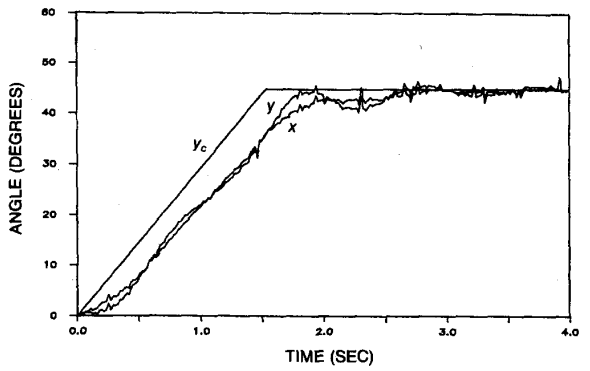

Fig. 13. Response of forward path P-D system.

degree-of-freedom model of the arm flexibility, predicted accurately the results obtained from most of the experiments. Basing flexible manipulator control software on these simplified models can lessen the computational overhead of a robot control system and allow effective real-time control with a minimum of exotic hardware or machine code programming [11].

References

[1] J.-N. Juang, L. G. Horta, and H. H. Robertshaw, "A Slewing Control Experiment for Flexible Structures," *J. Guid., Contr., Dynam.*, vol. 9, no. 5, pp. 599–607, 1986.

[2] T. E. Alberts, S. L. Dickerson, and W. J. Book, "Modeling and Control of Flexible Manipulators," Society of Manufacturing Engineers, Dearborn, MI, TP MS85-524, 1985.

[3] H. Kanoh, S. Tzafestas, H. G. Lee, and J. Kalat, "Modelling and Control of Flexible Robot Arms," *Proc. 25th Conf. on Decision and Control*, Athens, Greece, pp. 1866–1870, 1986.

[4] J. Tlusty and E. Stern, "Use of a Structural Model in Compensating for Robot Deflections," *Annals CIRP*, vol. 34, no. 1, pp. 357–363, 1985.

[5] J. G. Bollinger and N. A. Duffie, *Computer Control of Machines and Processes*, New York: Addison-Wesley, 1988.

[6] Y. Morimoto, T. Inamura, and K. Mizoguchi, "Dynamic Control of a Flexible Robot Arm by Using Experimental Modal Analysis," *Modeling and Control of Robotic Manipulators and Manufacturing Processes*, Boston, MA: ASME, pp. 337–343, 1987.

[7] G. Hastings and W. J. Book, "A Linear Dynamic Model for Flexible Robotic Manipulators," *IEEE Contr. Syst. Mag.*, vol. 7, no. 1, pp. 61–64, Feb. 1987.

[8] F. S. Tse, I. E. Morse, and R. T. Hinkle, *Mechanical Vibrations Theory and Applications*, Boston, MA: Allyn and Bacon, 1978.

[9] R. P. Paul, *Robot Manipulators: Mathematics, Programming and Control*, Cambridge, MA: MIT Press, 1981.

[10] D. Tesar and G. K. Matthew, *The Dynamic Synthesis, Analysis and Design of Modeled Cam Systems*, Lexington, MA: D. C. Heath & Co., 1976.

[11] R. L. Wells, "Feedforward and Feedback Strategies Applied to Controlling a Servo-Driven Flexible Arm," Master's Thesis, Univ. of Florida, Gainesville, FL, Aug. 1988.

Robert L. Wells earned the B.S. degree in mechanical engineering from the University of South Florida at Tampa in 1985. For several years prior, he worked in the contract engineering industry as a Senior Mechanical Designer. In 1988, he received the M.S. degree in mechanical engineering from the University of Florida at Gainesville, specializing in controls, and is presently pursuing a Ph.D. degree in the area of design and optimization.

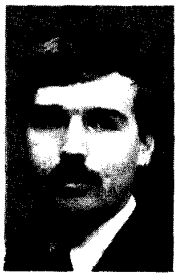

John K. Schueller holds degrees in mechanical engineering and agricultural engineering from Marquette University and Purdue University. Dr. Schueller is currently Associate Professor of Mechanical Engineering at the University of Florida. He has previously pursued his interests in the application of computers and control theory to manufacturing and agricultural machinery in positions at Gilson Brothers Co., Texas A&M University, and the Texas Agricultural Experimental Station. Dr. Schueller has received research grants from NASA, USDA, Deutz-Allis, Intel, and others.

Jiri Tlusty was educated in Czechoslovakia, where he earned his Doctor of Science degree in mechanical engineering in 1968 from the Technical University at Prague. He is Graduate Research Professor of Mechanical Engineering at the University of Florida, where he established the Machine Tool Laboratory and teaches courses in production engineering and structural dynamics. He has worked as Director of Research at VUOSO in Prague, Research Fellow at the University of Manchester, United Kingdom, and Professor of Mechanical Engineering at McMaster University in Ontario, Canada. He has received the SME Gold Medal and the ASME Centennial Medal, and is a past president of CIRP and NAMRI.